CHARACTERIZING DAMAGE EVOLUTION AND YIELD IN SANDSTONE UNDER TRIAXIAL LOADING AS A FUNCTION OF VARIOUS EFFECTIVE PRESSURE

A Thesis

by

ROBERT CHARLES CHOENS II

Submitted to the Office of Graduate Studies of
Texas A&M University
in partial fulfillment of the requirements for the degree of

MASTER OF SCIENCE

December 2009

Major Subject: Geology

CHARACTERIZING DAMAGE EVOLUTION AND YIELD IN SANDSTONE UNDER TRIAXIAL LOADING AS A FUNCTION OF VARIOUS EFFECTIVE PRESSURE

A Thesis

by

ROBERT CHARLES CHOENS II

Submitted to the Office of Graduate Studies of
Texas A&M University
in partial fulfillment of the requirements for the degree of

MASTER OF SCIENCE

Approved by:

Chair of Committee,	Frederick M. Chester
Committee Members,	Judith Chester
	Thomas Lalk
	Charles Bollfrass
Head of Department,	Andreas Kronenberg

December 2009

Major Subject: Geology

ABSTRACT

Characterizing Damage Evolution and Yield in Sandstone Under Triaxial Loading as a Function of Various Effective Pressure. (December 2009)

Robert Charles Choens II, B.S.E, University of Pennsylvania

Chair of Advisory Committee: Dr. Frederick Chester

Granular porous material is idealized as an elastic-plastic material, where macroscopic failure occurs at a critical stress by localized dilatant shear at low effective pressure and compactional cataclastic flow at high effective pressure. Yielding and accumulation of microscopic damage at sub-critical stress levels however also are important characteristic of the failure process. Here, load-reload triaxial compression tests are used to investigate damage development at low and high effective pressures, and validate prevailing models for failure across the brittle-ductile transition. Water saturated cylinders of Berea sandstone (18% porosity, 185μm grain size) were deformed at an axial strain rate of $4x10^{-5}$ s^{-1} to $8x10^{-5}$ s^{-1} pore pressures of 10, 20, and 30 MPa, and confining pressures of 50, 180, and 260 MPa to investigate the brittle, transitional, and ductile regimes. Measurement of sample strain and acoustic emissions are used to quantify the accumulation of damage and map equivalent damage states in stress space. Results illustrate that contours of equivalent damage for sub-critical stress states between yield and macroscopic failure are sub-parallel to the failure envelope across the brittle-ductile transition. Damage induced at one effective pressure (low, intermediate, or high pressure) has a systematic, but variable effect on failure at other effective pressure

conditions, supporting the concept of distinct processes and damage development in the low and high pressure regimes. Reloaded samples in the low pressure regime with an initial loading in the high pressure regime are significantly weakened, but reloaded samples in the high pressure regime are unaffected by an initial loading in the high pressure regime. The behavior across the brittle-ductile transition is most consistent with a model based on two distinct yield envelopes, each associated with distinct damage mechanisms and a sharp transition between the low and high pressure regimes.

TABLE OF CONTENTS

Page

LIST OF FIGURES

LIST OF TABLES

1. INTRODUCTION

Failure of a granular porous material is commonly idealized as that of an elastic plastic material characterized by two plastic end-member behaviors. Localized dilatant shear at low confining pressure and distributed cataclastic flow at high confining pressure, represented by the Mohr-Coulomb and elliptical cap failure envelopes [*Wong et al.*, 1997], respectively (Figure 1). There are other possibilities for failure envelopes based off different failure criterion: the Hoek-Brown, the modified Lade, the modified Wiebols-Cook, the Drucker-Prager, the Mogi, the Cam-Clay, and the modified Cam-Clay criterion [*Colmenares and Zoback*, 2002; *Zoback*, 2007]. Each end member behavior is associated with particular failure micromechanisms: failure at low effective pressure, P_e, is by localized shear fracture resulting from intergranular cracking, breaking of cemented grain boundaries, grain boundary sliding and grain rotation where increasing effective pressure increases normal stress at grain contacts, strengthening the frictional contacts; failure at high P_e occurs by distributed cataclastic flow resulting from intragranular fracture at Hertzian grain contacts, collapse of porosity, and grain rearrangement, where increasing effective pressure increases normal stress and stress concentrations at grain contacts, reducing the differential load needed to initiate intragranular cracking [*Menendez et al.*, 1996]. Experiments have demonstrated a transitional regime between the two end members that shows a combination of localized shear and distributed cataclastic flow [*Handin et al.*, 1963]. Previous studies have found

---

This thesis follows the style of *Journal of Geophysical Research.*

significant amounts of grain rotation and grain fracture in deformed samples that lead to either a localized diffuse compacting band composed of shear fractures and concentrated grain fracturing over a width of many grains or discrete compacting band with concentrated grain fracturing confined to only a few grain widths, with a dependence on grain size, grain sorting, cementation, and sample geometry [*Baud et al.*, 2004; *Besuelle et al.*, 2003; *Digiovanni et al.*, 2007; *Holcomb and Olsson*, 2003].

Yield and failure of a rock are two distinct phenomena. Yielding is defined as the deviation from elastic behavior and the onset of plastic deformation during loading, often involving cracking and acoustic emission [*Holcomb and Costin*, 1986]. After yielding, accumulation of damage occurs by micromechanisms corresponding to the confining pressure: breaking of cemented contacts, intergranular fracture, intragranular fracture, grain rotation and pore collapse. The yield surface defines the boundary between recoverable deformation and permanent deformation, and in terms of stress state, can be defined as a function of mean stress (p) and differential stress (q), and the internal damage state of the rock (α_κ), $F(p, q, \alpha_\kappa)=0$ [*Rudnicki*, 2004]. For constant α_κ, the yield surface may be defined uniquely by q and p in stress space. After yielding, the internal damage state increases so the shape of the yield surfaces evolves during loading. Failure of a rock can be defined as the ultimate strength in the brittle field where there is a loss of load bearing capability, the stress state where localization or macroscopic deformation occurs, the deviation from hydrostatic loading based on volumetric strain, or the highest rate of acoustic emissions during loading [*Fjaer et al.*, 2008; *Wong et al.*, 1997] . The failure envelope defines the boundary in stress space between an intact

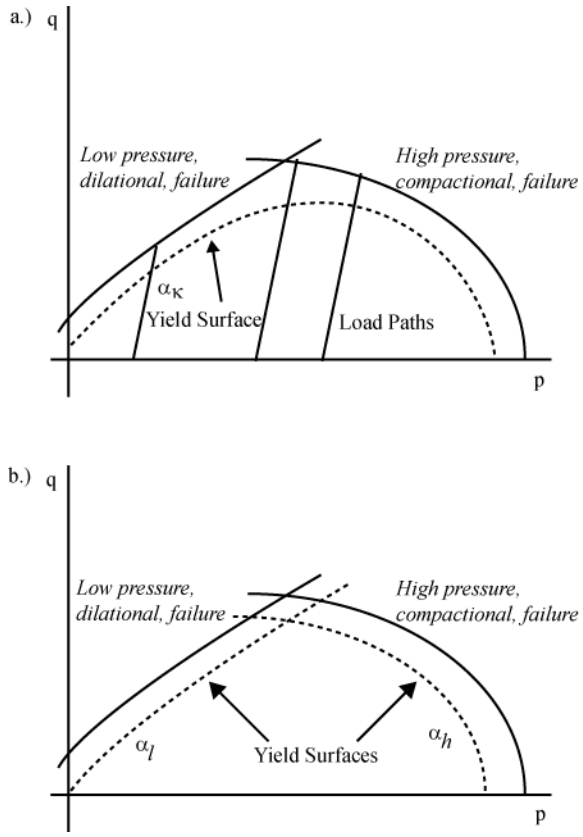

Figure 1. Experimental load paths mapped in Q-P space, differential stress v. mean stress. The solid black lines represent the failure envelope, the dashed lines represent the yield surfaces. A.) The yield surface is a single continuous surface. B.) The yield surfaces are composed of a combination of the Mohr-Coulomb envelope and the elliptical cap model, with a combination of the two in the transitional regime.

condition and failed conditions. It has been assumed that the yield surface has a similar shape to the failure envelope, but this is not necessarily true as the failure envelope is dependent on the accumulation of inelastic damage [*Rudnicki*, 2004].

It is unclear exactly how to account for multiple deformation mechanisms when modeling the yielding and failure of porous rocks. As an extension of bifurcation analysis, some authors have analyzed the conditions for localization in dilatant and compaction failure using a single yield surface, or a combination of two surfaces, one for shear and one for compaction [*Baud et al.*, 2006; *Challa and Issen*, 2004; *Issen and Rudnicki*, 2001; *Rudnicki*, 2004]. Issen and Rudnicki (2001) argue that a single yield surface is inadequate because there are two different micromechanisms responsible for yield. Two yield surfaces, intersecting at a convex vertex are necessary to model the two mechanisms, particularly in the complicated transitional regime [*Issen*, 2002]. Rudnicki (2004) points out that despite the fact that there are two different regimes, the evolution of the yield surface itself is not connected to the responsible micromechanisms; i.e. the yield surface is essentially a phenomenological description. Limited experimental data from compaction bands are better modeled by the two surface model [*Baud et al.*, 2006; *Issen*, 2002; *Wong et al.*, 2001], but this does not preclude using a single surface to describe the results. Existing microstructural data do not further elucidate the matter. Even though different micromechanisms are responsible for damage in the two regimes, both regimes show a similar anisotropic fracture fabric with respect to the maximum principal compressive stress [*Menendez et al.*, 1996]. Observations also show that grain crushing, an important micromechanism in the cap, also occurs past peak strength in

samples that have failed by shear localization [*Menendez et al.*, 1996]. If the micromechanisms operate across a wide section of the failure envelope and display smooth transitions in behavior, then a single yield surface may be sufficient to describe the yield behavior of a porous granular medium. In contrast, if the micromechanisms evolve in a fundamentally different way, with a sharp transition in between, then a two-mechanism yield envelope is necessitated [*Rudnicki*, 2004].

If distinct micromechanisms are active during yielding and leading up to failure at different pressures, then there should be distinct types of associated damage in each sub-critical stress state region. We hypothesize that if each region is characterized by distinct types of damage, then the ultimate macroscopic yielding and failure behavior of a rock will depends on the load path to failure and cumulative state of damage. Furthermore, not all damage is equal, for example, grain crushing induced at high confining pressures in the cap may have a significant impact on subsequent failure in the brittle regime; whereas, cracking first induced in the brittle regime, may be less significant to subsequent failure at the high confining pressures in the cap. These findings will be used to determine an appropriate yield surface model. Here, descriptions and results from a series of triaxial experiments on Berea sandstone are presented to characterize yield, damage development, and failure across the brittle-ductile transition. Single and multicycle loading paths were used to investigate the relative role of different macroscopic deformations mechanisms active during yielding and at failure under different effective pressure conditions. The results will be discussed in the context of previous microstructural work to determine relationships between

deformation mechanisms and pressure regimes, the effect of load path, and a descriptive yield surface model.

2. EXPERIMENTAL METHODOLOGY

Sample Description

Samples were cored from a single block of Berea Sandstones taken from the Cleveland Rock Quarry in Ohio. Previous studies on samples from this block have shown that the grain size, porosity, and mineralogy are comparable to published measurements for Berea [*Bobich*, 2005; *Menendez et al.*, 1996; *Zhang et al.*, 1990]. In general, the samples consist of subangular, well-sorted grains composed of 75-80% quartz, and 20-25% feldspar, as lesser amounts dolomite, rutile, zircon, kaolinite, and some secondary minerals [*Bobich*, 2005; *Zhang et al.*, 1990]. Dolomite grains and cement (up to 400μm) are distributed throughout the granular mass. Porosity measurements attained from mass differences between dry samples and samples saturated with alcohol or distilled waters range from 16-19%. The Schwawrtz-Saltykov method [*Hillard and Lawson*, 2003] was used to determine the grain size distribution from measurements of grain diameter in plane petrographic sections; the mean diameter is 185 μm [*Bobich*, 2005]. Bedding laminae are defined by mafic minerals visible on the hand sample scale, with spacing around 0.5 mm. Previous studies on Berea have shown that the laminations pronounced influence on fracture behavior [*Herrin*, 2008]. Samples were cored perpendicular to the laminations to minimize possible effects. Three different sizes of cores were used so as to not exceed the load capacity of the apparatus at the different confining pressures used in the experiments: 47.6 mm diameter cores were used for the low P_e regime, 38 mm for the transitional regime, and 25.3 mm for the high P_e regime, with lengths equal to twice the diameter. Ends were ground to produce

perfect right cylinders. Sample were isolated from the confining fluid by four layers of heat shrink polyolefin tubing and sealed at the pistons with nickel-chrome tie wires. Samples were soaked overnight in distilled water under a vacuum to ensure saturation.

Experimental Procedure

Samples were deformed in the Large Sample Rig (LSR) in the John Handin Rock Deformation Laboratory at Texas A&M University, College Station. The SLR is a gear driven, conventional triaxial apparatus that uses a liquid confining medium consisting of a kerosene-oil mixture, and an independent pore fluid pressure system [*Handin et al.*, 1972]. Ends of the sample were coated with molykote, a graphite lubricant, to reduce shear tractions at the piston interfaces. Experiments were run at room temperature and at a constant axial shortening rate of 2 μm/s. Axial shortening was measured with an accuracy of 0.01 mm outside the pressure vessel with a displacement transducer (DCDT) mounted between the moving piston and a fixed platen. Axial force was measured with an external load cell with an accuracy of 1kN. Pore pressure was maintained constant throughout the experiments to ensure fully drained conditions. Pore volume change was recorded by the displacement of the pore pressure generator using a DCDT, this change was used to calculate volumetric and radial strain. Acoustic emission (AE) was monitored during the experiment with a piezoelectric transducer (PZT) transfixed to the load cell situated against the upper piston. Signals from the PZT were conditioned with an amplifier and filter to reduce noise and obtain individual counts of AE.

Different load paths were explored in three suites of tests. The first suite of experiments, the single-load experiments, shortened undeformed samples under constant

confining pressure and pore pressure, well past failure to determine baseline mechanical and AE behavior. In the brittle regime, samples were subjected to a confining pressure of 50 MPa, and the pore pressures of 10, 20, or 30 MPa. In the transitional regime, the confining pressure was 180 MPa and the pore pressure 20 MPA. In the compactive regime, the confining pressure was 260 MPa and the pore pressure was 20 MPa.

The second suite of experiments involved two cycles of triaxial loading in the same pressure regime. The first cycle loaded an undeformed sample to establish a damaged state, followed by a second cycle of deformation on the same sample to determine the local slope of the yield surface reflecting the Kaiser effect. The Kaiser effect is a particular response in acoustic emissions (AE) resulting from reapplication of stress to a previous stressed brittle solid, such as a rock. This effect was first discovered by Joseph Kaiser in tensile tests on metals, alloys, and organic materials such as wood [*Holcomb*, 1993; *Kaiser*, 1950]. The general observation is that after a sample has been loaded and unloaded once, the rate of AE during reload abruptly increases when the maximum stress level previously achieved is reached a second time. The abrupt change in rate of AE often is called the Kaiser step, and the stress level at the step is the Kaiser stress. For the first cycle, an effective confining pressure of 30, 160, or 240 MPa (Pc=50, 180, or 260 MPa, Pp=20 MPa) was established, then the sample was loaded under triaxial compression to 75% of the failure strength for an hour duration, followed by removal of the differential load. For the second cycle, the effective confining pressure was increased or decreased by 10 MPa via a change in the pore fluid pressure, and then

the sample was reloaded under a compressive stress state through failure at constant effective confining pressure.

The third suite of experiments involved two cycles of loading, but in this case the effective pressure was changed by a greater amount such that the second cycle of loading occurred in a new pressure regime. This suite was designed to understand the yield surface at the boundary between two regimes. The first loading cycle involved establishing an effective pressure at 30, 160, or 240 MPa, application of compressional loading up to approximately 75% of the failure strength, holding that load for an hour duration, followed by unloading the differential force. For the second cycle, the effective pressure was changed via a change in the confining pressure to that of a different regime, while holding the pore pressure at constant 20 MPa, and then reloading the samples under triaxial compression to failure.

Macroscopic failure was determined by the slope of the differential stress versus axial strain curve to ensure consistent determinations across the brittle-ductile transition. Failure is defined by the point where the tangent slope of the stress-strain curve, normalized by the Young's modulus, equals 20%. In the two suites of experiments involving cyclic loading, the yield surface is identified on the basis of the Kaiser effect. Herein, the Kaiser step is interpreted to reflect the yield surface, and the onset of plastic damage is used to determine loads representing equivalent damage states [*Holcomb*, 1992]. Two different variations of the Kaiser step were recorded, the onset of AE activity during reloading of the experiments, as well as an abrupt change in AE rate

indicated by a change in slope of the cumulative AE rate versus differential strain curve, (Figure 2) [*Lavrov*, 2003].

In this paper we adopt the convention that compressive stresses and compactive strains are positive. We will note the maximum and minimum principal stresses by σ_1 and σ_3, respectively. The effective pressure, P_e, is defined as the difference between the confining pressure, P_c, and pore pressure, P_p. The effective mean stress, $(\sigma_1 + \sigma_3)/3 - P_p$, is denoted by P, and the differential stress, $\sigma_1 - \sigma_3$, by Q.

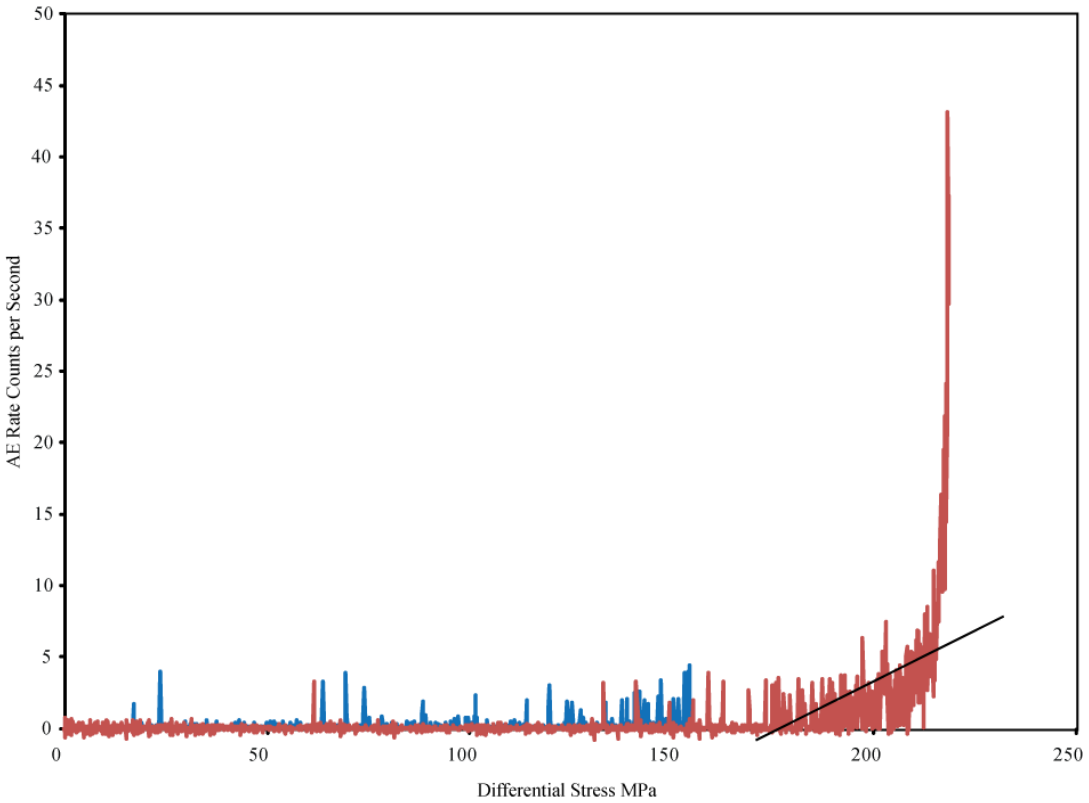

Figure 2. An example of the Kaiser step of a low P_e sample. AE rates versus differential stress for the load and reloads paths for a single sample. Blue represents the initial loading at 30 MPa P_e. Red represents the reloading of that samples at 40 MPa P_e. The black line indicates the onset of AE rate.

3. RESULTS

Single Load Experiments

In the low P_e regime (20, 30, and 40 MPa P_e), Berea sandstone exhibits classic dilatant shear failure at stress conditions described by the Mohr-Coulomb failure envelope (Figure 3). Failure is expressed by the formation of shear fractures oriented approximately 30° to the σ_1 axis.

The sample deformed in the high P_e regime (240 MPa P_e) is characterized by mechanically ductile behavior with strain hardening and volumetric compaction (Figure 3). The high P_e experiments display a few small stress drops; these likely reflect o-ring extrusion. Samples show distributed damage and radial expansion.

The experiment in the transitional regime (160 MPa P_e) displays mechanically ductile behavior with post failure softening and volumetric compaction (Figure 3). The sample display a slight bulge over about three fourths of the length, and is cut by several small conjugate shears inclined at 45° to the σ_1 axis.

Assuming cumulative AE counts are a proxy for inelastic strain, the AE number may be used to determine relative damage states. The AE count is normalized by the cumulative count at failure to determine damage relative to damage states at failure, and to compare damage states between experiments deformed along different load paths (Table 1). Relative damage states determined for experiments at different P_e are contoured in stress space to infer the form of the yield surface across the brittle-ductile transition (Figure 4). Equivalent damage states, i.e. points on a yield surface, suggest that the yield surface mimic the form of the failure envelope (Figure 4).

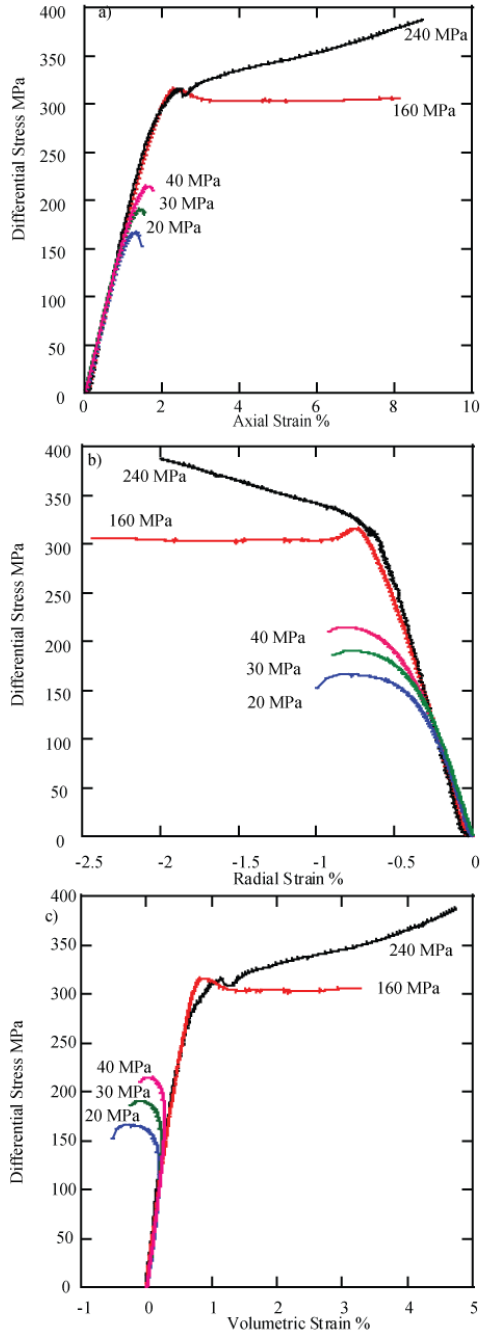

Figure 3. Results from the single load experiments for effective confining pressures of 20, 30, 40, 160, and 240 MPa. (a) Differential stress versus axial strain. (b) Differential stress versus radial strain. (c) Differential stress versus volumetric strain.

TABLE 1. Percentages of AE at yield for single load experiments

exp #	1%	5%	10%	25%	50%	75%	90%	yield	Pe MPa
4954	14.34	28.54	88.18	127.92	149.37	160.04	163.56	164.17	20
normed	8.73%	17.38%	53.71%	77.92%	90.99%	97.49%	99.63%	100.00%	
4952	42.25	82.51	117.58	154.41	177.88	185.71	187.82	188.68	30
normed	22.39%	43.73%	62.32%	81.84%	94.27%	98.42%	99.54%	100.00%	
4970	53.16	138.65	163.02	191.10	207.02	211.76	212.95	213.27	40
normed	24.93%	65.01%	76.44%	89.60%	97.07%	99.29%	99.85%	100.00%	
5004	166.11	240.71	267.25	292.47	304.89	310.63	312.50	313.63	160
normed	52.96%	76.75%	85.21%	93.25%	97.21%	99.04%	99.64%	100.00%	
4995	185.02	241.69	257.87	277.48	292.31	303.05	308.70	311.06	240
normed	59.48%	77.70%	82.90%	89.20%	93.97%	97.42%	99.24%	100.00%	

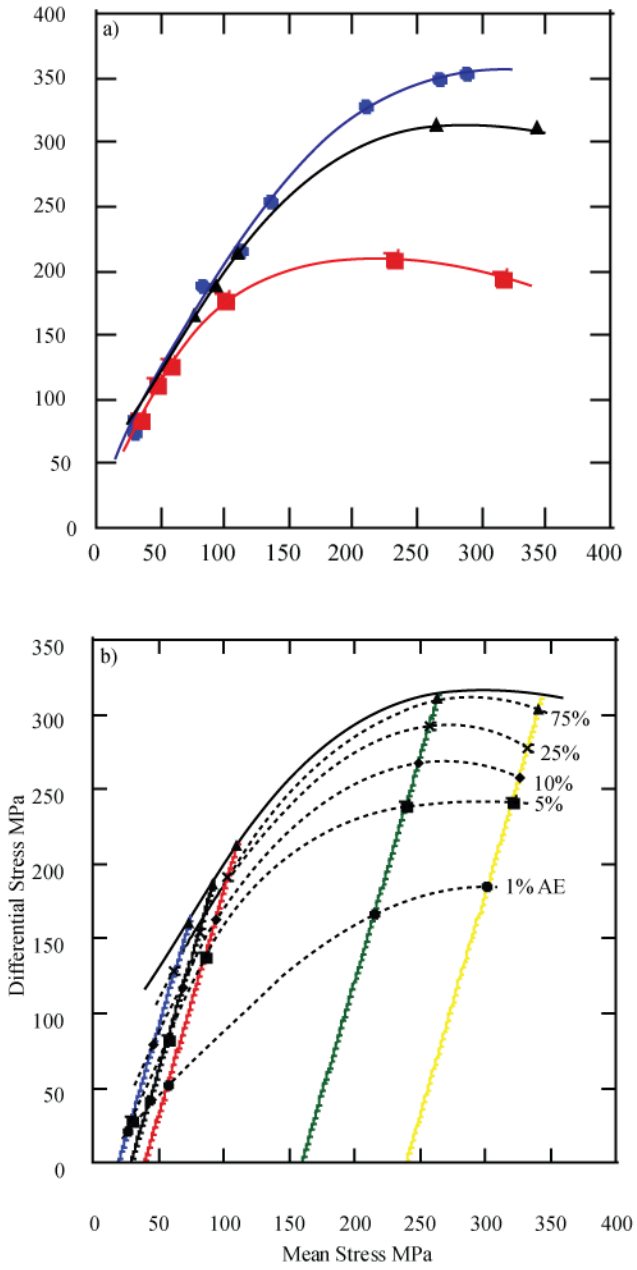

Figure 4. Equivalent damage contours. a) A comparison of failure envelopes for Berea sandstone. Blue circles represents results dry Berea samples deformed at 10-4 s-1 from Bobich, 2005; red squares represent results from Wong et al, 1997; and black triangles represent results from this study of saturated Berea deformed at 10-5 s-1. b) Results from the single load experiments plotted in terms of differential stress versus mean stress. Blue represents a load at 20 MPa effective pressure; black, 30 MPa; red, 40 MPa; green, 160 MPa; yellow, 240 MPa. Dashed lines represent values of AE normalized to the counts at failure for each experiment. Values of 1, 5, 10, 25, and 75 are indicated on the plot. The curved black line represents the failure envelope.

Load-Reload Experiments in the Same Pressure Regime

Reloaded samples in the low P_e regime appear to have a slightly lower failure strength compared to the single load samples at the same P_e, but this may not be significant given the sample to sample variability seen for Berea sandstone (Figure 5). Samples all developed fractures at 30° to the σ_1 axis.

Reloaded samples in the high P_e regime show slight strengthening compared to the single load samples and a decrease in failure strength with increasing P_e. Samples show no signs of fracture or bulging, just uniform axial shortening.

Reloaded samples in the transitional regime show slight softening compared to the single load samples, and a slight decrease in failure strength with increasing confining pressure. Whereas the AE rate for the single load and reload tests are similar in the low and high P_e regimes, the transitional regime displays a qualitatively different AE response. With increasing P_e, there is an increase in AE rate. The experiments at 150 and 160 MPa P_e show a post-peak plateau in AE rate that is missing in the experiment at 170 MPa P_e. The 170 MPa P_e experiment also undergoes significantly more strain hardening than the other two experiments, perhaps indicating a more compactional response. The sample reloaded at 150 MPa P_e shows slight bulging in the lower half of the sample and is cut by high angle conjugate shears. The sample reloaded at 170 MPa displays relatively distributed damage and slight bulging over the length of the sample. Fractures inclined 45° to the σ_1 axis are present, but are small and non-pervasive. Structures that look like compaction bands are also present along some bedding planes.

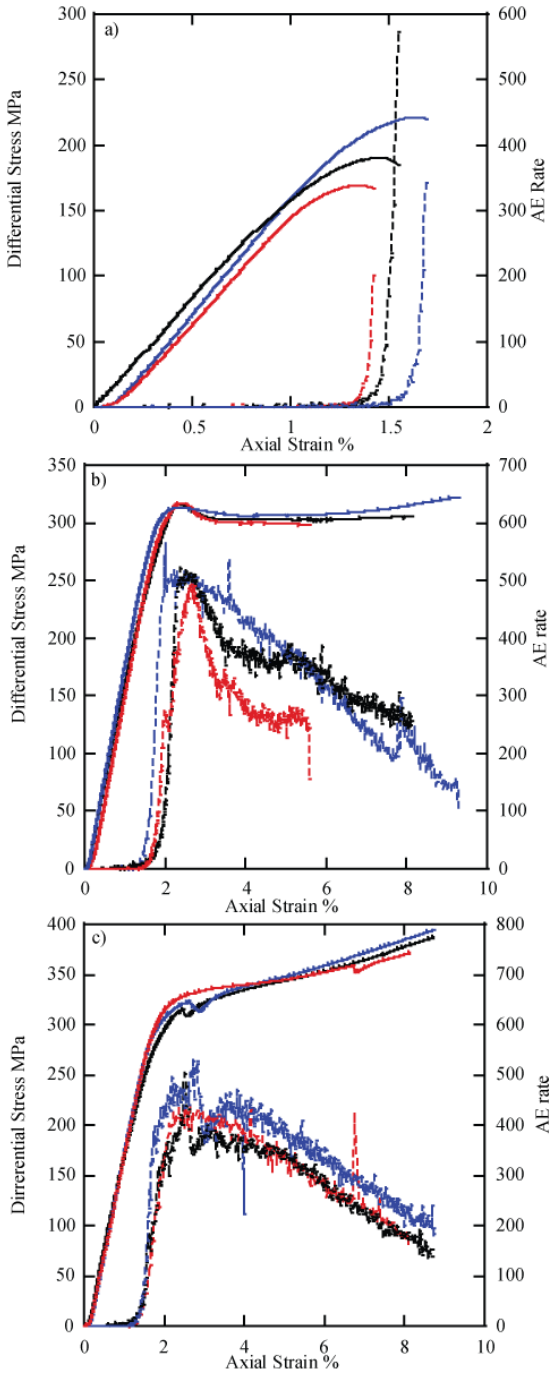

Figure 5. Differential stress (MPa) and AE rate (counts/sec) versus axial strain (%) curves for load-reload experiments. Solid lines represent differential stress, dashed lines represent AE rate. a) Low effective pressure regime. Red represents 20 MPa effective pressure; black, 30 MPa; blue, 40 MPa. b) Intermediate effective pressure regime. Red represents 150 MPa effective pressure; black, 160 MPa; blue, 170 MPa. c) High effective pressure regime. Red represents 230 MPa effective pressure; black, 250 MPa; blue, 240 MPa.

Using AE counts to identify the Kaiser step and onset of inelastic damage during reload tests allows the determination of the local slope of the yield surface (Figure 6, Table 2). Because each reload follows an initial load to a known stress and damage state, the stress at the Kaiser step and the peak stress in the initial load cycle should have equivalent damage states, and thus determines the local slope of the yield surface. The local slope generally is consistent with the failure envelope. In the low P_e regime, the local yield surface has a positive slope, and is subparallel to the failure envelope. In the transitional regime, the yield surface and failure surface are both subhorizontal. However, in the high P_e regime, the failure envelope is still subhorizontal while the local yield surface has a negative slope. The local slope of the yield surface also agrees with the results from the equivalent damage states for the low P_e and transitional regime, as slopes for the damage states are positive and subhorizontal, respectively (Figure 5). The slope of the equivalent damage contour, however, is subhorizontal, whereas the local slope of the yield surface is negative.

Sequential Loading in Different Pressure Regimes

Reloading at low P_e. An initial stage of compression in the intermediate P_e regime does not effect a significant change in sample strength for reloading in the low P_e regime. In contrast, samples are significantly weaker during reloading at low P_e, if first subjected to compression at high P_e (Figure 7a). All samples reloaded to failure under low P_e develop a fracture that is oriented 30° to the σ_1 axis.

Reloading at high P_e. An initial stage of compression to yield in the intermediate P_e regime strengthens samples, as illustrated by strain hardening behavior in the post

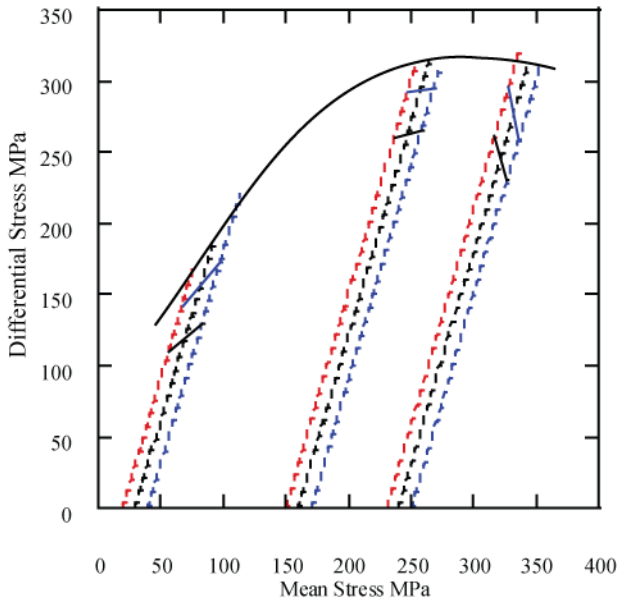

Figure 6. Local slopes of yield surfaces. Results from the load-reload experiments in q-p space. Dashed black curves represent single load experiments at 200 bars pore pressure; red represents reloads at 300 bars pore pressure; blue, 100 bars pore pressure. Solid black lines represent the onset of AE in the reloads; solid blue lines, the inflection point in AE. The curved black line represents the failure envelope.

TABLE 2. Listing of Loads and Kaiser steps for Reload Experiments

exp #	load	onset	knee	yield	load-reload Pe
4959	153	110	142	220	30-40 MPa
normed	81.09%	50.03%	64.59%	100.00%	
4960	152	130	173	168	30-20 MPa
normed	80.56%	77.22%	102.77%	100.00%	
5006	245	260	292.5	314	160-150 MPa
normed	78.12%	82.88%	93.24%	100.00%	
5009	246	265	295	308	160-170 MPa
normed	78.44%	85.97%	95.70%	100.00%	
4996	245	261	296	320	240-230 MPa
normed	78.76%	81.60%	92.55%	100.00%	
4997	250	230	258	309	240-250 MPa
normed	80.37%	74.34%	83.40%	100.00%	
5024	156	282	296	312	30-160 MPa
normed	82.68%	90.50%	94.99%	100.00%	
5003	152	240	287	304	30-240 MPa
normed	80.56%	78.90%	94.35%	100.00%	
5010	246	172	180.5	188	160-30 MPa
normed	78.44%	91.49%	96.01%	100.00%	
5020	245	236	272	318	160-240 MPa
normed	78.12%	74.21%	85.53%	100.00%	
5017	250	143	156	164	240-30 MPa
normed	80.37%	87.25%	95.18%	100.00%	
5018	250	266	291	306	240-160 MPa
normed	80.37%	86.93%	95.10%	100.00%	

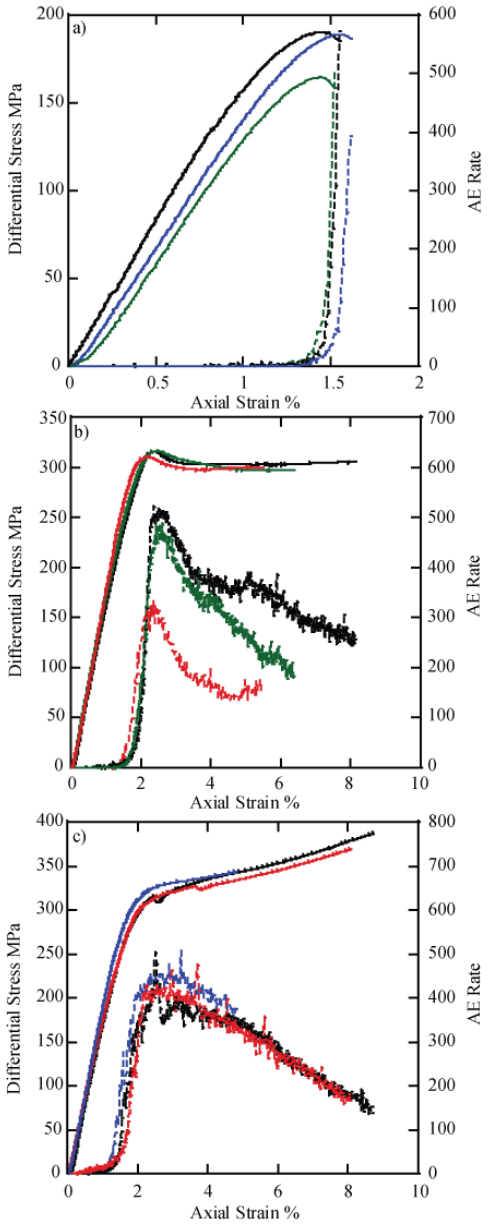

Figure 7. Differential stress (MPa) and AE rate (counts per second) versus axial strain (%) for regime change experiments. Solid lines represent differential stress; dashed lines, AE rate. a) Low effective pressure regime. Black curves represent the single load experiment at 30 MPa Pe; blue represents the reload experiment at 30 MPa Pe with an initial load at 160 MPa; green, reload from 240 MPa. b) Intermediate effective pressure regime. Black curves represent the single load experiment at 160 MPa; red represents the reload experiment at 160 MPa from an initial load at 30 MPs; blue, reload from 240 MPa. c) High confining pressure regime. Black represents the single load experiment at 240 MPa; red represents the reload at 240 MPa from an initial load of 30 MPa; blue, reload from 160 MPa.

yield phase during reloading at high P_e. In contrast, samples show little change in mechanical behavior during reloading at high P_e, if first subjected to yield under low P_e conditions (Figure 7c). This low P_e-high P_e sample develops faint, thin, localized, high-angle conjugate fractures.

Reloaded samples in the high P_e show that an initial load at 160 MPa P_e strengthened the sample for the reload relative to the undeformed sample. In contrast, the initial load at 30 MPa appears to have had very little effect on the behavior during the reload relative to that of the undeformed sample. The reload with an initial load at 160 MPa P_e has less strain hardening post yield compared to the other two experiments. This sample also displays signs of what could be faint, small, non pervasive high angle conjugate fractures whereas the samples from the other experiments show no signs of localization.

Reloading at intermediate P_e. Samples reloaded at intermediate P_e are not influenced significantly by a preloading phase at low or high P_e (Figure 7b).The sample initially loaded at 30 MPa P_e shows significantly lower AE rate when compared to the other tests (Figure 7b). The sample with an initial load at 30 MPa displays a bulge in the top and bottom third of the sample, where faint, non-pervasive, small, high-angle conjugate fractures formed. An apparent compaction band, along a bedding plane, occurs in the middle of the sample. Bulging occurred over half of the sample that was initially loaded at 240 MPa P_e; the bulged region displays faint, small, non-pervasive, high-angle conjugate fractures, as well as some possible compaction bands localized along bedding planes.

For all reload tests, the onset of AE is delayed significantly, relative to AE behavior during the initial loading of the undeformed rock (Figure 8). Furthermore, the onset of AE in samples initially loaded at a lower effective P_e is delayed further than those initially loaded at a higher P_e (Table 2).

Radial strain, ε_r, was calculated for each experiment from the measurements of total volume strain, ε_v, and axial strain, ε_a, where $\varepsilon_v=2\varepsilon_r+\varepsilon_a$. From these strains, Young's modulus, E, and the Poisson's ratio, ν, were determined from the elastic portion of the stress-strain data. Elastic parameters were determined for samples from both the initial load and the reload portions of the tests. The mean and standard deviation of the elastic moduli were determined for the undeformed rock samples, at a given P_e, and compared against the elastic moduli for reloaded samples. In the brittle regime, initial loading at 160 and 240 MPa P_e statistically changes the elastic moduli of the reloaded sample (Figure 9, Table 3). In both cases, samples were significantly softer. In the transitional regime, initial loading at 240 MPa P_e results in a stiffer response upon reload, whereas initial loading at 30 MPa P_e has no affect on the stiffness. In the high P_e regime, initial loading at 160 MPa P_e significantly stiffens the rock, but loading at 30 MPa P_e has no affect.

Plastic volumetric strain, ε_{vp}, was determined from the total volume strain, ε_v, and the elastic volume strain, ε_{ve}, where $\varepsilon_v=\varepsilon_{ve}+\varepsilon_{vp}$. ε_{ve} was calculated from the initial linear gradient in the differential stress versus total volume strain curve, and then extrapolated throughout the loading. Initial loading significantly softens the samples for subsequent deformation in the low P_e regime; this is particularly true for the sample

initially loaded at 240 MPa P_e. Upon reloading, plastic strain occurs earlier and samples accumulate volume strain at a faster rate (Figure 10a). Reloading samples in the high P_e regime illustrates that an initial stage of loading at intermediate P_e strengthens the sample to subsequent deformation, reducing the total volume strain, whereas an initial loading at 30 MPa P_e softens the sample. The initial loading at 160 MPa P_e does not affect the onset of plastic volume strain in the reloaded sample, but it does retard the evolution of plastic volume strain (Figure 10b). In the transitional regime, initial loading in the high P_e regime significantly strengthens the sample, reducing the accumulated volume strain. The pre-loading phase also greatly delays the onset of plastic volume strain. In contrast, initial loading to yield at 30 MPa has no affect on the evolution of volume strain for reloading at intermediate or high P_e conditions (Figure 10c).

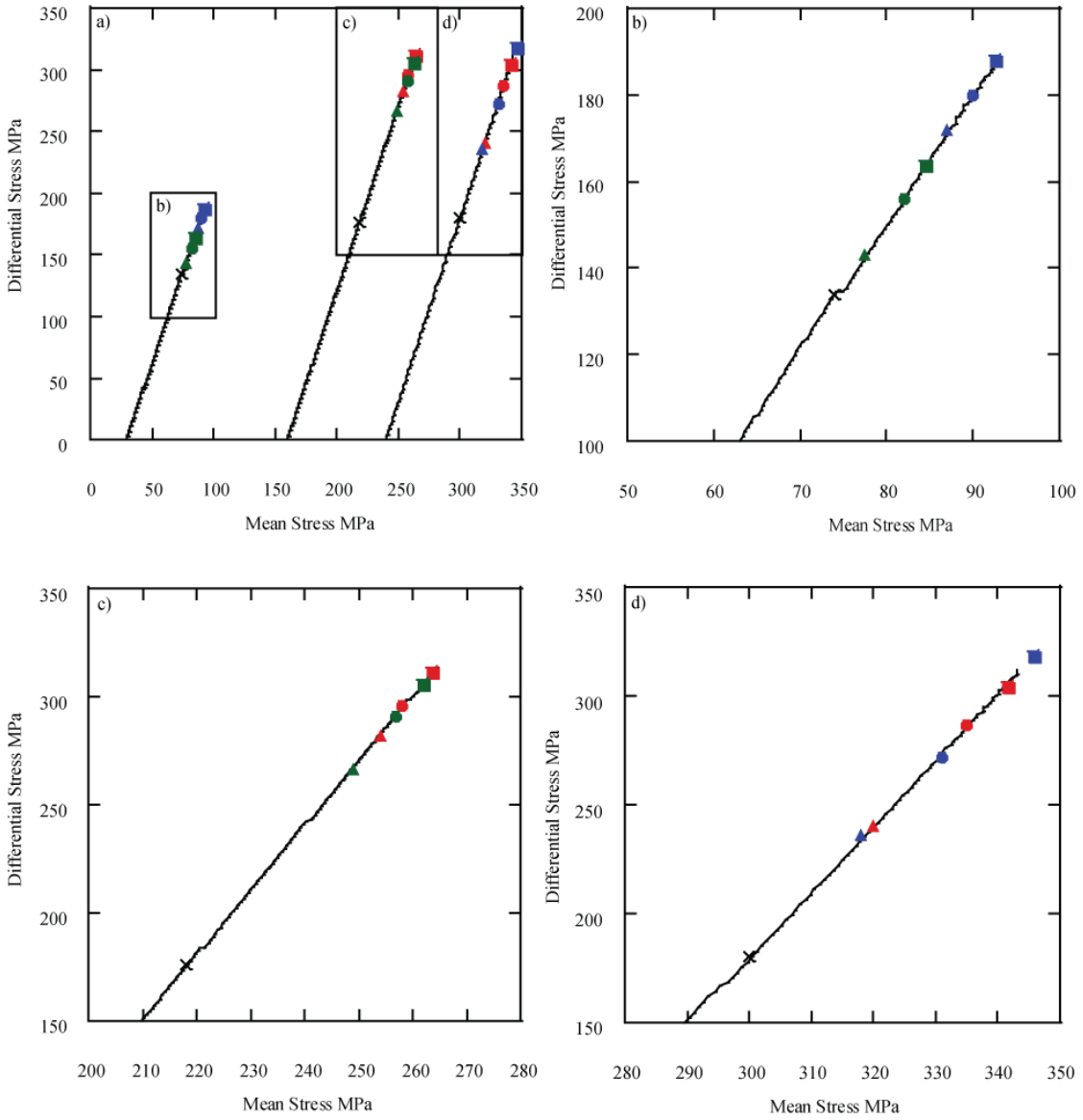

Figure 8. Kaiser steps in regime change experiments. Results of the regime change experiments plotted in Q-P space. a) Black curves represent the single load experiments, black X's correspond to onset of AE in the single load experiments; red represents reloads with an initial loading at the low Pe; blue represents reloads with an initial loading at the intermediate Pe; green represents reloads with and initial loading at high Pe. Triangles represent the onset of AE in the reloads, circles represent the inflexion point in AE, and squares represent the yield stresses in the reloads. The black rectangles represent the area shown in parts b-d. b) Enlargement of low Pe conditions. c) Enlargement of intermediate Pe. d) Enlargement of high Pe.

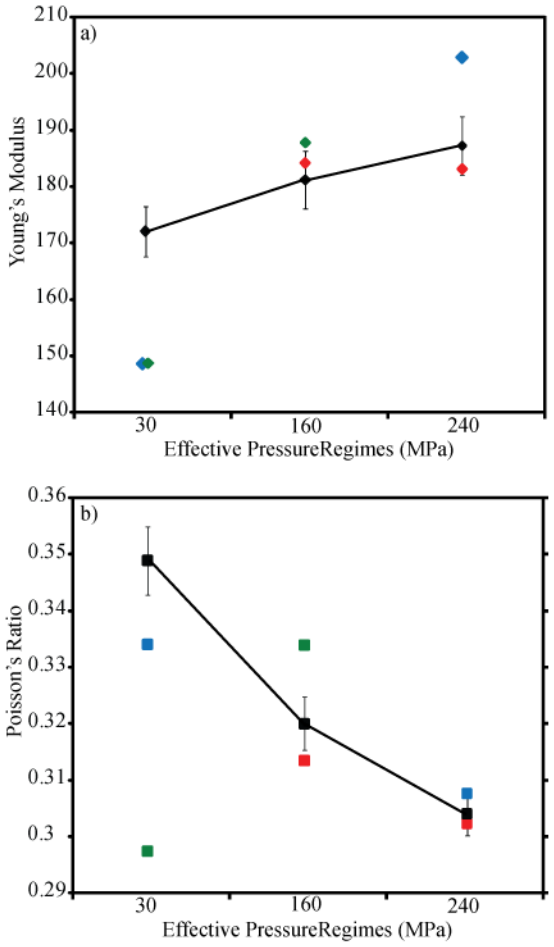

Figure 9. Young's modulus (MPa) and Poisson's ratio versus effective pressure regimes (MPa) for single load and regime change experiments. Black represents single load results, red represents reloads with an initial loading at 30 MPa effective pressure, blue represents reloads with an initial loading at 160 MPa, and green represents reloads with an initial loading at 240 MPa. Uncertainty bars represent a standard deviation from an average of single load results and initial load paths. a) Young's modulus versus effective pressure. b) Poisson's Ration versus effective pressure.

TABLE 3. Elastic Moduli for each experiment. An L after the experimental number indicates it is the load portion of the experiment. Highlighted rows indicate reload experiments.

exp #	E	ν	Pe bars
4954	170.81	0.35	200
4960r	165.76	0.35	
4952	168.23	0.36	300
5036	180.66	0.35	
4959 L	169.64	0.34	
4960 L	170.15	0.35	
5024 L	171.57	0.35	
5003 L	172.26	0.34	
mean	172.09	0.35	
stnd dev	4.44	0.01	
5010	148.67	0.33	at I
5017	148.66	0.30	at H
4970	169.59	0.34	400
4959	179.48	0.36	
5006	186.17	0.35	1500
5004	180.51	0.31	1600
5006 L	178.18	0.32	
5009 L	183.90	0.33	
5010 L	175.03	0.32	
5020 L	188.40	0.32	
mean	181.20	0.32	
stnd dev	5.17	0.00	
5024	184.16	0.31	at L
5018	187.74	0.33	at H
5009	195.41	0.36	1700
4996	197.43	0.35	2300
4995	193.10	0.31	2400
4996 L	189.34	0.31	
4997 L	190.93	0.30	
4998 L	173.47	0.31	
5017 L	186.08	0.30	
5018 L	190.31	0.30	
mean	187.21	0.30	
stnd dev	7.11	0.00	
5003	183.14	0.30	at L
5020	202.90	0.31	at I
4997	204.12	0.34	2500

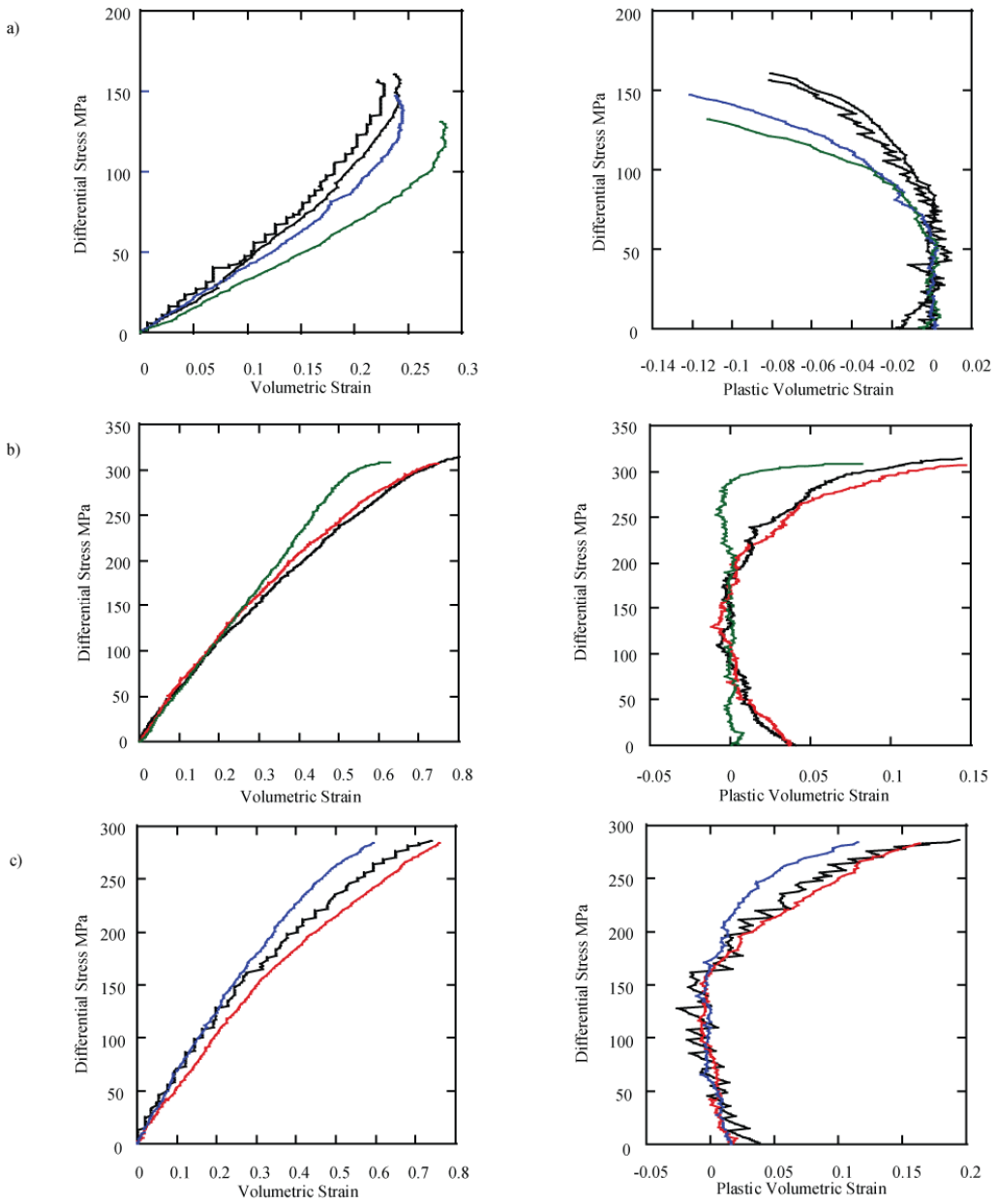

Figure 10. Volume strain analysis. The left column is differential stress (MPa) versus volumetric strain (%), and the right column is differential stress (MPa) versus plastic volumetric strain (%). Solid lines represent single load experiments, dashed lines are reload experiments. a) 30 MPa Pe regime. Black lines are single load experiments, blue represents the reload from an initial load at 160 MPa Pe; green, reload from 240 MPa Pe. b) 160 MPa Pe regime. Black represents single load experiments. Red represents the reload from an initial load at 30 MPa Pe; green, reload from 240 MPa Pe. c) 240 MPa Pe regime. Black represents single load experiments. Red represents reload from an initial load of 30 MPa Pe; blue, reload from 160 Mpa Pe.

4. DISCUSSION

Similarity of Yield Surfaces and Failure Envelopes

It is well established that the failure strength of porous granular rock varies systematically with confining pressure. The Mohr-Coulomb criterion describes failure in the brittle regime and a cap describes failure in the compactive regime [*Handin et al.*, 1963; *Wong et al.*, 1997]. The AE data presented in Figures 4 and 6 support the assumption that the yield surfaces vary in a similar fashion as the failure envelope. In the brittle regime, the slopes of the AE contours are strongly positive and parallel to the failure envelope. Connecting the brittle to transitional regime, the contours are less positive but still are parallel to the failure envelope. From the transitional to compactive regime, the contours are horizontal to subhorizontal and parallel to subparallel to the failure envelope. Even though different mechanical processes are responsible for damage in the experiments, i.e., dilatant processes in the brittle regime, and compactive processes in the transitional and compactive regimes, these data suggest that the amount of post-yield damage evolves in a similar fashion across the brittle-ductile transition (Figure 6).

The failure envelopes in the reload experiments show a positive slope in the brittle regime, a subhorizontal to negative slope in the transitional regime, and a negative slope in the compactive regime. In each regime, the yield surfaces are subparallel to the failure envelope, with a positive slope in the brittle regime, a subhorizontal to positive slope in the transitional regime, and a negative slope in the compactive field. This is a good verification that the mechanisms responsible for yield have the same relationship

with changing P_e as macroscopic failure. The positive slope of the Kaiser envelope in the brittle regime suggests that the same mechanisms responsible for macroscopic failure are also responsible for yield: intergranular cracking, breaking of cemented grain boundaries, intergranular slip, and grain rotation. The negative slope of the yield surface in the compactive regime suggests that the same mechanisms responsible for macroscopic failure are also responsible for yield: fracture of grains initiating at Hertzian grain contacts, collapse of porosity, and grain rearrangement. The subhorizontal yield surface and failure envelope in the transitional regime suggest that there is a combination of two end member mechanisms active. The slight positive slope of the yield surface would suggest a larger contribution from brittle mechanisms responsible for yield while the slight negative slope of the failure envelope would suggest that ultimately compactive processes are controlling macroscopic yield. The fact that the slope of the yield surface is much more negative than the failure envelope indicates that the failure mechanisms are still in transition, and some brittle mechanisms are active in failure while yield is completely high P_e mechanisms. The sharp difference in yield surfaces between the transition and high P_e regimes indicates a much sharper transition between the yield mechanisms than failure mechanisms. This difference in slope between the failure envelope and yield surface could also indicate that in the high P_e regime the yield surfaces are not parallel to the failure envelope in the cap.

Our findings are consistent with cyclic load tests and the Kaiser effect demonstrated for low porosity Tennessee marble [*Holcomb*, 1992]. Cyclic load tests and the Kaiser effect were used to determine the slope of the yield surface, the ultimate

strength envelope, and the initial yield surface for intact, undeformed rock. Very similar to the results presented here from the load-reload experiments. In marble, Holcomb found a bilinear failure envelope with different slopes for damage surfaces. For low confining pressure, the damage surfaces paralleled the failure envelope. At higher confining pressures, the damage surface depended on the initial load. At low initial loads, the damage surface had negative to subhorizontal slope. With increasing load, the slope of the damage surface increased, but never to that of the failure envelope. In our experiments, the yield surface defined by cyclic loading at high initial loads is parallel to the failure envelope except for the high P_e. It is interesting to note that Holcomb found different slopes between the failure envelope and onset of yield determined by onset of AE in undeformed rocks, whereas AE behavior in our single load experiments mimicked failure (Figure 4). This is an interesting result because Holcomb found that Tennessee marble developed a horizontal slope that transitioned into a negative slope to AE onset yield surface, despite the fact Tennessee marble is low porosity and does not have a negative slope to the failure envelope. He hypothesized that the horizontal slope was due to a change in mechanisms, from cracking to twinning, but did not understand the mechanics behind the negative slope. It is possible that twinning produces far less AE than cracking, so picking the AE onset based on AE rate changes would artificially reduce the AE onset because of the comparatively fewer counts. The transition in Berea sandstone would be from grain boundary to grain breakage, which has higher AE signal so this problem does not manifest itself in our experiments.

Low and High Pressure Yielding Processes and Damage Development

AE results from single load and load-reload experiments demonstrate that damage accumulate in a similar proportion across the brittle-ductile transition, but the load-reload experiments involving a regime change show that damage induced at the high and low pressures are not equivalent. The damage produced during initial loading in the transitional and compactive regimes has a large influence on the development of plastic volumetric strain in the brittle regime, but the damage induced in the brittle regime has little to no affect on the transitional and compactive volumetric strain (Figure 10). Similar trends are also illustrated in the behavior of elastic moduli (Figure 9, Table 3). The moduli demonstrate that the damage induced in the transitional and compactive regimes statistically changed the moduli in the reloaded samples in the brittle regime, but the damage induced in the brittle regime did not have a statistically significant effect on the moduli in the reloaded samples in the transitional and compactive regimes. The differential stress versus axial strain curves also reinforce this trend (Figure 7). In the brittle regime, the reload with a loading in the compactive regime fails at a much lower stress than the single load experiment, but in the compactive regime the reloaded sample with an initial reloading in the brittle regime is identical to the single load experiment.

These trends agree quite strongly with the observations and models in Menendez et al. (1996). In the brittle regime they found the sample failed by a localized shear fracture and yielded by distributed intergranular cracking, breaking of cemented grain boundaries, grain boundary sliding and grain rotation. Close to peak stress, isolated patches experience grain fracturing, and an incipient fracture occurs by the coalescence

of these patches into an isolated shear fracture that propagates throughout the rock [*Lockner et al.*, 1992; *Menendez et al.*, 1996]. Here the yield mechanisms are not the ultimate responsible mechanisms of failure as additional mechanisms are active in the creation of a shear fracture. In the compactive regime, they found the sample failed by distributed cataclastic flow accomplished by intragranular cracking at Hertzian grain contacts, collapse of porosity, and grain rearrangement, where the mechanisms responsible for failure are the same mechanisms responsible for yield.

These micromechanical behaviors explain the difference in damage induced in low P_e versus high P_e regimes. In the low P_e regime, yield is accomplished by the fracturing of cemented grain boundaries, intergranular slip on inclined boundaries and subsequent dilation. The higher confining pressures in high P_e regimes negate this type of damage. The increased confining pressure increases the normal stresses at grain contacts preventing further intergranular slip and essentially closes any previously fractured grain boundaries. In the high P_e regime, yield is accomplished by distributed intragranular fracturing initiating at Hertzian contacts. Individual grains fail throughout the sample, essentially weakening the matrix of the rock as intact grains are reduced and non-cohesive surfaces are increased. During the reload at the low P_e regime, the increased non-cohesive surfaces are now pervasive from the samples so it is easier to activate intergranular slip and dilate vulnerable cracks. Less differential stress is required to cause damage, so the sample is softer as shown by the elastic moduli and volumetric strain curves and fails at a lower stress than expected. The reduced confining pressure in the low P_e regime exacerbates the damage caused in the high P_e regime and

demonstrates the importance of load path and the cumulative damage state on macroscopic behavior.

This behavior could also be understood in terms of the failure criterion and yield surface function, $F(p, q, \alpha_\kappa)=0$ [*Rudnicki*, 2004]. From the relationships observed in the experiments, it appears that there would be several yield surfaces corresponding to the different micromechanisms, one for intergranular (grain boundary) cracking (α_1), one for intragranular cracking at Hertzian contacts (α_2), and one for porosity collapse (α_3) (Figure 11). Both intergranular and intragranular cracks produce new cohesionless grain surfaces that are available for slip. The increased number of potential frictional sliding surfaces facilitates intergranular slip and dilation during reloading under low effective pressures. Intergranular cracking would be active in the low P_e regime and intragranular cracking would be active in the high P_e regime. In addition, the high P_e regime would also have an additional element of damage, porosity collapse. Yielding in the high pressure regime would contain both elements of damage, in intragranular cracks and porosity collapse, that would affect reloading in the low pressure regime, but yielding in the low pressure regime does not produce that additional element of porosity collapse so it would have no demonstrable effect on reloading in the high pressure regime. From the local yield surface data (Figure 6), the intergranular cracking envelope would be parallel to the failure envelope, but the high P_e surfaces might not be parallel to the failure envelope as indicated by the steeper slope of the local yield surface.

The fact that the initial loading in the brittle regime further delays the onset of AE more than initial loading under transitional and compactive conditions, but does not

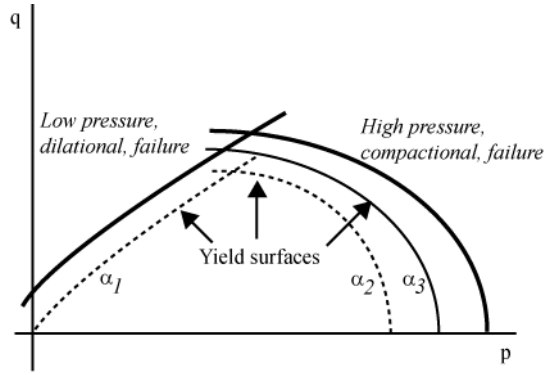

Figure 11. Failure envelopes and yield surfaces in stress space. Dark black lines represent failure envelopes, dashes black lines and the thin black lines represent yield surfaces. a1 represents the yield surface corresponding to grain boundary cracking, a2 represents the yield surface corresponding to fracturing of grains at Hertzian contacts, and a3 represents the yield surface corresponding to porosity collapse.

affect the mechanical behavior of the reloaded samples (Figures 7-10), agrees with the interpreted micromechanical behavior based on Menendez et al. (1996). In the low P_e regime, when damage is accomplished by intergranular fracture, that breaks cemented grain boundaries, and intergranular slip, the grain boundaries most likely to separate and slip at the beginning stages of yielding are the weakest boundaries, i.e., the grains with the fewest contacts, the least amount of or weakest cement. Preferential intragranular cracking will occur along pre-existing flaws that are aligned with the σ_1 axis. So during initial loading in the brittle regime, these vulnerable grains break their cemented boundaries and slip on that new surface, relieving the stress concentrations for that particular grain. During unloading of the differential load and subsequent increase of the effective pressure, the slipped grains get locked into place. When the sample is reloaded at the higher effective pressure, the vulnerable grains that would be the first to crack have already slipped and are locked into a new lower stress position. As the load increases, new grains become vulnerable and crack just as expected in an undeformed sample. The effect is only evident at the initial stages of yield, delaying the onset of AE. This does not affect the mechanical behavior because of the disproportionate cumulative AE between the low and high P_e samples. The high P_e regime has two orders of magnitude more cracking than the low P_e regime. So this phenomena only manifests subtly in the delay of the onset of AE, and is soon negated by the higher levels of cracking that takes place at higher pressure.

Processes and Damage Development in the Transitional Regime

In the transitional regime, macroscopic failure is manifested by a combination of brittle and compactive mechanisms. At the macroscopic scale, samples from the transitional field bulge by the formation of high angle conjugate shear bands. Based on the microstructural observations of Menendez et al. (1996), we know that the distributed deformation of the samples reflect grain rearrangement and a reduction in porosity that are facilitated by fracturing under Hertzian-type stressing at grain-grain contact junctions, sliding on grain boundary surfaces, and rotation and translation of grains. These microstructural processes would lead to similar volumetric strain behavior (Figure 10) and display similar elastic moduli (Figure 9, Table 3) when deformed in the transitional and high P_e regime. In the low P_e regime, the reloaded samples with initial loadings at the transitional and compactive regimes show advanced plastic strain and a statistically lower elastic moduli. In reloaded samples at the transitional regime, the initial loading at the brittle regime has no effect but the initial loading at the compactive regime greatly delays the onset of plastic strain. The elastic moduli are also changed by the initial loading at the compactive regime but unaffected by the initial loading at the low P_e regime. In the reloaded samples in the high P_e regime, the initial loading in the low P_e regime has no effect but the initial loading at the transitional regime lessens the development of plastic strain. Moduli of the reloaded samples are also affected by the initial load in the transitional regime but not by the initial load in the low P_e regime. The transitional and compactive loads have the same effect on the low P_e regime and on each other, and the low P_e loads have no effect on the transitional and high P_e regime. This

would suggest that damage developed in the transitional regime is controlled by the high pressure mechanisms. Both the high and low pressure mechanisms are active, but the high pressure mechanisms are dominant.

In terms of the yield surfaces, this would indicate load paths intersecting the horizontal part of the failure envelope first intersect the yield surface for grain fracturing (Figure 11). The transition between the yield surfaces for intergranular and intragranular cracking would be lower pressure than the transition in the failure envelope, most likely where the slope of the envelope is still positive. Yielding in the transitional regime would contain multiple elements of damage that would have mechanical effects in the low pressure regime, but yielding in the low pressure regime does not produce both types of damage so it would have little effect on reloading in the transitional regime. Because of the multiple mechanisms, the transitional regime and the high pressure regime have similar effects on each other.

This finding is in good agreement with previous microstructural work in *Baud et al.* (2004). Their study found the transitional regime in Berea, failure was marked by high angle conjugate shear zones and diffuse compaction bands. At the lower confining pressure end of the transitional regime, high angle conjugate shear bands formed near peak stressed that transitioned into diffuse compaction bands, creating stress strain curves and AE response similar to the experiments presented here. Microstructural observations confirmed that intense grain fracturing was focused inside the compaction bands and to a lesser extent along the periphery of the band. Away from the band, only the occasional intragranular cracks were noted. In the transitional regime, the

macroscopic failure is controlled by the high pressure mechanism. Yield is accomplished by localized patches high pressure mechanisms, and ultimately high pressure mechanisms dominate and control failure, even though shear bands would indicate some contribution from low pressure mechanisms. This is in agreement with the elastic moduli and volume strain data presented here (Figures 9, 10). *Baud et al*. (2004) found broad diffuse bands that reflected the coalescence of smaller discrete bands. Outside of the bands, grains are intact. In these instances, only the higher pressure mechanisms can be found in the transitional regime. It is interesting to note that *Digiovanni et al.* (2007) found both low pressure mechanisms and high pressure mechanisms active in their experiments on compaction bands in Castlegate sandstone. In diffuse compaction bands, damage manifested itself as intense grain crushing and porosity collapse, but between bands the porosity was reduced by grain rotation. This effect was obvious because Castlegate sandstone has maintained its pre-diagenetic fabric with angular grains, high porosity and sparse cementation. The authors hypothesized that grain rotation had not occurred in previous studies on Berea because of the higher degree of cementation and the more indurated fabric of the earlier samples. The higher confining pressures and higher normal stresses in the transitional regime in Berea also make it far less likely to have slip between grains as opposed to fracturing at grain contact junctions. It is also possible that intergranular slip occurred and was lost in comparison to the intense localized patches of intragranular cracking. Berea could yield by a combination of the low and high pressure mechanisms, with distributed low P_e mechanisms and localized areas of high P_e damage that ultimately dominate yielding and

control failure. If low P_e mechanisms are active, then that could explain the differences in local yield surface slopes between the transitional and high P_e regime (Figure 6). It is beyond the scope of this study to rule out the possibility of low pressure mechanisms in the transitional regime in Berea. It is apparent from the results presented here that in the transitional regime high pressures mechanisms dominate the macroscopic behavior. This would suggest the transition between Mohr-Coulomb and the cap is a fairly abrupt transition, which most likely occurs at a lower pressure than the onset of the horizontal slope.

5. SUMMARY AND CONCLUSIONS

The experimental data presented here demonstrates that yield surfaces are roughly parallel to the macroscopic failure envelope, and the accumulation of damage with triaxial loading is proportionally similar across the brittle-ductile transition. There is some evidence that yield surfaces in the high-pressure (cap) regime have significantly more negative slope compared to the failure envelope. Damage induced during yielding in the high-pressure compactional regime has a significant impact on subsequent yield and failure in the low-pressure regime, but damage induced in the brittle regime has little affect on yielding and failure in the compactional regime, i.e., high pressure damage mechanisms influence low pressure mechanisms, but not vice versa. It was also shown that in the transitional region where the slope of the yield envelope is approximately zero, high-pressure damage mechanisms dominate. There is little evidence that low-pressure mechanisms of damage are significant.

In conclusion, yield and failure are affected by load path. This is due to the differences in damage mechanisms. Both the low pressure and high pressure mechanisms create cohesionless boundaries, intergranular and intragranular cracking, respectively, but the high pressure regime contains additional elements of damage like porosity collapse. The most appropriate yield surface model to describe this would be a multiple yield surface model, with different surfaces for intergranular cracking, intragranular cracking, and porosity collapse. The yield surface for the intergranular cracking would be parallel to the failure envelope, but the yield surfaces for the intragranular and porosity collapse would deviate from the failure envelope. The

transition between low and high pressure yield surfaces is fairly abrupt and occurs at the low pressure region of the brittle-ductile transition, i.e., where the slope of the failure envelope is slightly positive.

REFERENCES

Baud, P., Klein, E., and T. F. Wong (2004), Compaction localization in porous sandstones: spatial evolution of damage and acoustic emission activity, *J. Struct. Geol.*, *26*(4), 603-624.

Baud, P., Vajdova, V., and T. F. Wong (2006), Shear-enhanced compaction and strain localization: Inelastic deformation and constitutive modeling of four porous sandstones, *J. Geophys. Res.-Solid Earth*, *111*(B12), 17.

Besuelle, P., Baud, P., and T. F. Wong (2003), Failure mode and spatial distribution of damage in Rothbach sandstone in the brittle-ductile transition, *Pure Appl. Geophys.*, *160*(5-6), 851-868.

Bobich, J. K. (2005), Experimental Analysis of the Extension to Shear Fracture Transition in Berea Sandstone, unpublished Master's thesis. Texas A&M University.

Challa, V., and K. A. Issen (2004), Conditions for compaction band formation in porous rock using a two-yield surface model, *J. Eng. Mech.-ASCE*, *130*(9), 1089-1097.

Colmenares, L. B., and M. D. Zoback (2002), A statistical evaluation of intact rock failure criteria constrained by polyaxial test data for five different rocks, *Int. J. Rock Mech. Min. Sci.*, *39*(6), 695-729.

Digiovanni, A. A., Fredrich J. T., Holcomb D. J., and W. A. Olsson (2007), Microscale damage evolution in compacting sandstone, in *The Relationship Between Damage and Localization*, pp. 89-103, Geological Society of London, London, United Kingdom.

Fjaer, E., Holt, R. M., Horsrud, P., Raaen A. M., and R. Risntes (2008), *Petroleum Related Rock Mechanics*, 2nd ed., Elsevier.

Handin, J., Hager, R., Friedman, M., and J. Feather (1963), Experimental deformation of sedimentary rocks under confining pressure; pore pressure tests, *Bulletin of the American Association of Petroleum Geologists*, *47*(5), 717-755.

Handin, J., Friedman, M., Logan, J. M., Pattison, L. J., and H. S. Swolfs (1972), Experimental folding of rocks under confining pressure: buckling of single layer rock beams., in *Flow and Fracture of Rocks (Griggs Volume)*, edited by H. C. Heard, et al., pp. 1-28, American Geophysical Union, Washington D.C.

Herrin, E. A. (2008), Experimental Study of Shear and Compaction Band Formation in Berea Sandstone, unpublished Master's thesis. Texas A&M University.

Hillard, J. E., and L. R. Lawson (2003), *Stereology and Stochastic Geometry*, Kluwer Academic Publishers, Dordrecht, The Netherlands.

Holcomb, D. J., and L. S. Costin (1986), Detecting damage surfaces in brittle materials using acoustic emissions, *J. Appl. Mech.-Trans. ASME*, *53*(3), 536-544.

Holcomb, D. J. (1992), Localization studies under triaxial conditions, in *Rock mechanics. Proc. of the 33rd U S symposium*, pp. 661-670, A.A Balkema, Rotterdam.

Holcomb, D. J. (1993), Observations of the Kaiser effect under multiaxial stress states - implications for its use in determining in-situ stress, *Geophysical Research Letters*, *20*(19), 2119-2122.

Holcomb, D. J., and W. A. Olsson (2003), Compaction localization and fluid flow, *J. Geophys. Res.-Solid Earth*, *108*(B6), 13.

Issen, K. A., and J. W. Rudnicki (2001), Theory of compaction bands in porous rock, *Phys. Chem. Earth Pt. A-Solid Earth Geod.*, *26*(1-2), 95-100.

Issen, K. A. (2002), The influence of constitutive models on localization conditions for porous rock, *Engineering Fracture Mechanics, 69,* 1891-1906.

Kaiser, J. (1950), An Investigation into the Occurrence of Noises in Tensile Tests of a Study of Acoustic Phenomena in *Tensile Tests, Tech. Hosch. Munchen, Munich, Germany*.

Lavrov, A. (2003), The Kaiser effect in rocks. Principles and stress estimation techniques, *International Journal of Rock Mechanics and Mining Sciences (1997)*, *40*(2), 151-171.

Lockner, D. A., Byerlee, J. D., Kuksenko, V., Ponomarev, A., and A. Sidorin (1992), Observations of quasistatic fault growth from acoustic emissions, in *Fault Mechanics and Transport Properties of Rocks: a Festschrift in Honor of W F Brace*, edited by B. Evans and T.-f. Wong, Acad Press, San Diego, CA,.

Menendez, B., Zhu, W. L., and T. F. Wong (1996), Micromechanics of brittle faulting and cataclastic flow in Berea sandstone, *J. Struct. Geol.*, *18*(1), 1-16.

Rudnicki, J. W. (2004), Shear and compaction band formation on an elliptic yield cap, *Journal of Geophysical Research, B, Solid Earth and Planets*.

Wong, T. F., David, C., and W. L. Zhu (1997), The transition from brittle faulting to cataclastic flow in porous sandstones: Mechanical deformation, *J. Geophys. Res.-Solid Earth*, *102*(B2), 3009-3025.

Wong, T. F., Baud, P., and E. Klein (2001), Localized failure modes in a compactant porous rock, *Geophys. Res. Lett.*, *28*(13), 2521-2524.

Zhang, J. X., Wong, T. F., Yanagidani, T., and D. M. Davis (1990), Pressure-induced microcracking and grain crushing in Berea and Boise sandstones - acoustic emission and quantitative microscopy measurements, *Mech. Mater.*, *9*(1), 1-15.

Zoback, M. D. (2007), *Reservoir Geomechanics*, Cambridge University Press, Cambridge, UK.

VITA

ROBERT CHARLES CHOENS II
M.T. Halbouty Building, College Station, TX 77843
rcchoens@neo.tamu.edu

Education

Texas A&M University, College Station, TX, M.S., Structural Geology, December 2009
Thesis: Characterizing Damage Evolution and Yield in Sandstone Under Triaxial Loading as a Function of Changing Effective Pressure
Advisor: Dr. Frederick M. Chester

University of Pennsylvania, Philadelphia, PA, B.S.E., Mechanical Engineering, May 2007

Honors and Awards

Mel and Debby Friedman Scholarship, Texas A&M University, Fall 2008
Conoco Phillips Fellowship, Texas A&M University, 2007- 2008. 2009-2010
ConocoPhillips SPIRIT Scholarship, Texas A&M University, 2008-2010

Publications

Abstracts

Choens, R. C., Chester, F. M. (2009) Characterizing Damage Evolution and Yield in Sandstone Under Triaxial Loading as a Function of Changing Effective Pressure. AGU Annual Convention and Exhibition Denver, June 7-10.

Choens, R. C., Chester, F. M. (2009) Characterizing Damage Evolution and Yield in Sandstone Under Triaxial Loading as a Function of Changing Effective Pressure. AAPG Annual Convention and Exhibition Denver, June 7-10.

Professional Associations

AAPG, Fall 2007-present
AGU, Fall 2009-present
SPE, Summer 2009-present
Geosciences Dean's Student Council, Fall 2008-Spring 2009
-Geology and Geophysics Graduate Student Representative
American Society of Mechanical Engineers, 2004-2007
-University of Pennsylvania Chapter Class Representative